MICROCOPY RESOLUTION TEST CHART
NATIONAL BUREAU OF STANDARDS-1963-A

DAVID W. TAYLOR NAVAL SHIP RESEARCH AND DEVELOPMENT CENTER

Bethesda, Md.   20084

ON THE EVALUATION OF AXISYMMETRIC FOREBODY SHAPES FOR
DELAYING LAMINAR-TURBULENT TRANSITION — PART I:
BACKGROUND AND ANALYSIS OF THE PROBLEM

by

Mario J. Casarella, John T.C. Shen and

Brian E. Bowers

APPROVED FOR PUBLIC RELEASE: DISTRIBUTION UNLIMITED

DTIC

FEB 1 3 1986

E

SHIP ACOUSTICS DEPARTMENT
RESEARCH AND DEVELOPMENT REPORT
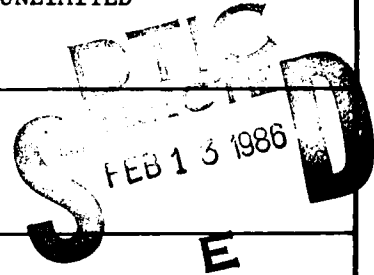
August 1977   Report 77-0074

MAJOR DTNSRDC ORGANIZATIONAL COMPONENTS

DTNSRDC COMMANDER 00 TECHNICAL DIRECTOR 01	
OFFICER-IN-CHARGE CARDEROCK 05	OFFICER-IN-CHARGE ANNAPOLIS 04
SYSTEMS DEVELOPMENT DEPARTMENT 11	
SHIP PERFORMANCE DEPARTMENT 15	AVIATION AND SURFACE EFFECTS DEPARTMENT 16
STRUCTURES DEPARTMENT 17	COMPUTATION, MATHEMATICS AND LOGISTICS DEPARTMENT 18
SHIP ACOUSTICS DEPARTMENT 19	PROPULSION AND AUXILIARY SYSTEMS DEPARTMENT 27
MATERIALS DEPARTMENT 28	CENTRAL INSTRUMENTATION DEPARTMENT 29

SECURITY CLASSIFICATION OF THIS PAGE (When Data Entered)

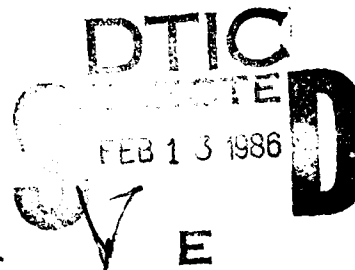| REPORT DOCUMENTATION PAGE		READ INSTRUCTIONS BEFORE COMPLETING FORM
1. REPORT NUMBER DTNSRDC 77-0074	2. GOVT ACCESSION NO. ADA 164135	3. RECIPIENT'S CATALOG NUMBER
4. TITLE (and Subtitle) ON THE EVALUATION OF AXISYMMETRIC FOREBODY SHAPES FOR DELAYING LAMINAR-TURBULENT TRANSITION - PART I: BACKGROUND AND ANALYSIS OF THE PROBLEM		5. TYPE OF REPORT & PERIOD COVERED Formal Report
		6. PERFORMING ORG. REPORT NUMBER
7. AUTHOR(s) Mario J. Casarella, John T.C. Shen and Brian E. Bowers		8. CONTRACT OR GRANT NUMBER(s)
9. PERFORMING ORGANIZATION NAME AND ADDRESS David W. Taylor Naval Ship Research and Development Center Bethesda, Maryland 20084		10. PROGRAM ELEMENT, PROJECT, TASK AREA & WORK UNIT NUMBERS (See reverse side)
11. CONTROLLING OFFICE NAME AND ADDRESS Naval Sea Systems Command Code 037 Washington, D.C. 20362		12. REPORT DATE August 1977
		13. NUMBER OF PAGES 42
14. MONITORING AGENCY NAME & ADDRESS(if different from Controlling Office)		15. SECURITY CLASS. (of this report) UNCLASSIFIED
		15a. DECLASSIFICATION/DOWNGRADING SCHEDULE

16. DISTRIBUTION STATEMENT (of this Report)

APPROVED FOR PUBLIC RELEASE: DISTRIBUTION UNLIMITED

17. DISTRIBUTION STATEMENT (of the abstract entered in Block 20, if different from Report)

18. SUPPLEMENTARY NOTES

19. KEY WORDS (Continue on reverse side if necessary and identify by block number)

Boundary-layer Transition
Axisymmetric Bodies
Optimal Shape
Laminar Flow

20. ABSTRACT (Continue on reverse side if necessary and identify by block number)

This investigation examines the inherent potential flows and laminar boundary layer characteristics on the nose surface of axisymmetric bodies that can postpone the natural transition process from a laminar to turbulent flow. Based on this analysis, an effort is made to find a correlation between the geometrical features of a given body shape, and the ability of that shape to delay transition. Ellipsoidal forebodies for which stability —
(Continued on reverse side)

DD FORM 1473 EDITION OF 1 NOV 65 IS OBSOLETE
1 JAN 73
S/N 0102-LF-014-6601

(Block 10)

    Task 18186, Program Element 62543N,
    Project F43.452 and
    Work Unit 1-1942-081

(Block 20 continued)

computations have been performed, are presented to show those
attributes of a good nose design. These examples give some
direction to future work in obtaining the optimal design.
    Prior to the discussion of the effects of nose shape on
transition, a brief review of the method commonly used for pre-
dicting transition is presented followed by a discussion of the
distinctive features of axisymmetric flows as compared to the
widely discussed two-dimensional flows. This is essential back-
ground material and forms the basis of most of the arguments
presented on the choice of a good bow shape design. Key,

Accession For		
NTIS GRA&I	☒	
DTIC TAB	☐	
Unannounced	☐	
Justification		
By		
Distribution/		
Availability Codes		
	Avail and/or	
Dist	Special	
A-1		

TABLE OF CONTENTS

LIST OF FIGURES

NOTATION

A	Amplitude of unstable disturbance during downstream growth
A_o	Initial amplitude of disturbance
C_p	Local pressure coefficient, $C_p = 1 - (\frac{U_e}{U_\infty})^2$
$C_{p_{min}}$	Minimum value of local pressure coefficient
D	Maximum diameter of axisymmetric body
M_2, M_3	Dimensionless pressure gradient for two-dimensional and axisymmetric flows defined by equations (A7) and (A12)
P_2, P_3	Function defined in Appendix A
$R(x)$	Function defined in Appendix A
R_D	Body Reynolds number, $R_D = \frac{DU_\infty}{\nu}$
R_L	Reynolds number, $R_L = \frac{LU_\infty}{\nu}$
R_{S_t}	Local Reynolds number, $R_{S_t} = \frac{S_t U_e(x)}{\nu}$
$R_{\delta*_3}$	Dimensionless displacement thickness, $R_{\delta*_3} = \frac{\delta*_3 U_e(x)}{\nu}$
$r_o(x)$	Local radial distance of axisymmetric body shape
s_3	Distance along axisymmetric body surface
s_2	Downstream distance for two-dimensional flow
(s_3, y_3)	Downstream and transverse coordinates for axisymmetric flow
(s_2, y_2)	Downstream and transverse coordinates for two-dimensional flow
S_t	Downstream distance locating the position of transition
$S_{p_{min}}$	Downstream distance locating the position of $C_{p_{min}}$
t	Subscript denoting transition
$u(\eta)$	Local velocity within the boundary layer region

v

$U_e(s)$	Local velocity at the edge of the boundary layer
U_∞	Uniform velocity upstream of body
x	Axial distance measured from stagnation point
ξ, η	Similarity variables defined in Appendix A
β	Dimensionless pressure gradient parameter defined in Appendix A
$\delta^*(\beta, \xi)$	Computed displacement thickness defined in Appendix A
δ^*_3	Displacement thickness for axisymmetric shape
δ^*_2	Displacement thickness for two-dimensional shape

ABSTRACT

This investigation examines the inherent potential flows and laminar boundary layer characteristics on the nose surface of axisymmetric bodies that can postpone the natural transition process from a laminar to turbulent flow. Based on this analysis, an effort is made to find a correlation between the geometrical features of a given body shape, and the ability of that shape to delay transition. Ellipsoidal forebodies for which stability computations have been performed, are presented to show those attributes of a good nose design. These examples give some direction to future work in obtaining the optimal design.

Prior to the discussion of the effects of nose shape on transition, a brief review of the method commonly used for predicting transition is presented followed by a discussion of the distinctive features of axisymmetric flows as compared to the widely discussed two-dimensional flows. This is essential background material and forms the basis of most of the arguments presented on the choice of a good bow shape design.

ADMINISTRATIVE INFORMATION

1

1.0 METHOD FOR PREDICTING TRANSITION

1.1 BACKGROUND

The development of the viscous boundary layer on the nose of an axisymmetric body normally starts at the stagnation point as a steady laminar flow growing in thickness along the downstream direction until irregular fluctuations or bursts appear causing the process of transition from the laminar to turbulent flow[1]. The transition process is caused by "instability" of the flow, that is, the tendency for small natural disturbances (due to noise, mechanical vibrations, surface roughness, non-uniformity of the oncoming stream, etc.) to be amplified into substantial fluctuations.

The classical method for predicting the location of transition is based on stability theory which attempts to predict if these natural disturbances, inherent in all flows, will grow or decay during the downstream development of the laminar boundary layer.

The analysis assumes that these disturbances are represented as infinitesimal two-dimensional velocity fluctuations

$$u' = \phi(y) \exp [i(\alpha x - \omega t)]$$

where $\alpha = \alpha_r + i\alpha_i$ - complex wave number of disturbance

$c = 2\pi\omega/\alpha_r$, phase velocity of wave

ω, circular frequency of wave

Instability of the flow occurs when the spatial amplification rate is positive or $\alpha_i < 0$, for which the disturbance begins to grow spatially in a complex three-dimensional manner until the eruption of a turbulent burst. The growth pattern of these discrete unstable waves can be

---

[1]DeMetz, F.C. and M.J. Casarella "An Experimental Study of the Intermittent Properties of the Boundary Layer Pressure Field During Transition on a Flat Plate," NSRDC Report 4140 (November 1973).

characterized by the spatial amplification ratio, $\ln(\frac{A}{A_o})$, which measures

the amplification from the initial instability (neutral stability point)

to the onset of burst eruptions. The Smith-Gamberoni method of predicting

transition is based on the criterion that the onset of bursting will occur

when $\ln(\frac{A}{A_o}) \approx 9\text{-}11$. However, the pioneering work by Granville[2] was the

first attempt at correlating the conditions of the flow instability with

the onset of fully turbulent flow. His work identified the inherent flow

characteristic that allow realistic predictions for a wide class of body

shapes.

It has been shown experimentally that these two-dimensional regular

waves do not properly represent the growth of the waves on axisymmetric

bodies prior to the breakdown of the flow into turbulent burst. Further-

more, the amplification ratio concept of predicting transition is based

strictly on linear stability theory for infinitesimal disturbances and

does not account for the actual phenomena of three-dimensionality, non-

linear interaction of the waves, and vortex breakdown. However, the

Smith-Gamberoni method appears to predict transition within a 20 per cent

range for low Reynolds number.

In order to predict the growth of the wave by this method and its

subsequent amplification rate when $\alpha_i < 0$, numerical solutions of the

eigenvalue problem posed by the Orr-Sommerfeld equations are required at

each station along the axisymmetric body surface. This requires a

significant amount of computational effort. The input for this program

requires knowing the laminar boundary layer velocity profile $(\frac{u}{U_e})$ and

---

[2]Granville, P.S., "The Calculation of the Viscous Drag of Bodies of
Revolution," DTMB Report No. 849 (July 1953).

the local displacement Reynolds number $R_{\delta^*_3}$ at each station along the axisymmetric body surface prior to the onset of transition.

The Smith-Gamberoni method of prediction, based on solutions of the Orr-Sommerfeld equation, is widely used because it reflects the best current state-of-the-art technique. The results appear to have some correlation with experimental results obtained in model testing at Reynolds numbers ($R_D = 8\text{-}10\text{x}10^6$). These values are significantly lower than those existing in an operational environment (e.g., $R_D = 50$ - 110×10^6). Experimental tests at higher Reynolds numbers, which are lacking, are required in order to gain confidence in the validity of the prediction technique for even the most conventional shaped bodies. However, the Smith-Gamberoni method can be used to make comparative evaluations of various shapes in order to gain insight into the so-called "best preliminary design." This is essentially the philosophy underlying the remarks contained in this report.

1.2 SUMMARY OF COMPUTATIONAL PROCEDURE

The overall algorithm for predicting the transition point is shown in Figure 1. Four distinct phases of the computational algorithm are required. These are shown schematically in Figure 1 and will be briefly discussed. Appendix A, which is a condensed version of the equations derived in Reference 3, contains the derivation and summary of the equation used in this discussion.

A. Axisymmetric Potential Flow Computation

By using the Neumann Program, the pressure distribution C_p and $\dfrac{U_e}{U_\infty}$

---

[3] Niedzwecki, J., "Laminar and Turbulent Incompressible Boundary Layers on Bodies of Revolution in Axial Flow," Doctoral Dissertation, Catholic University of America, Dept. of Mechanical Engineering (Feb 1977).
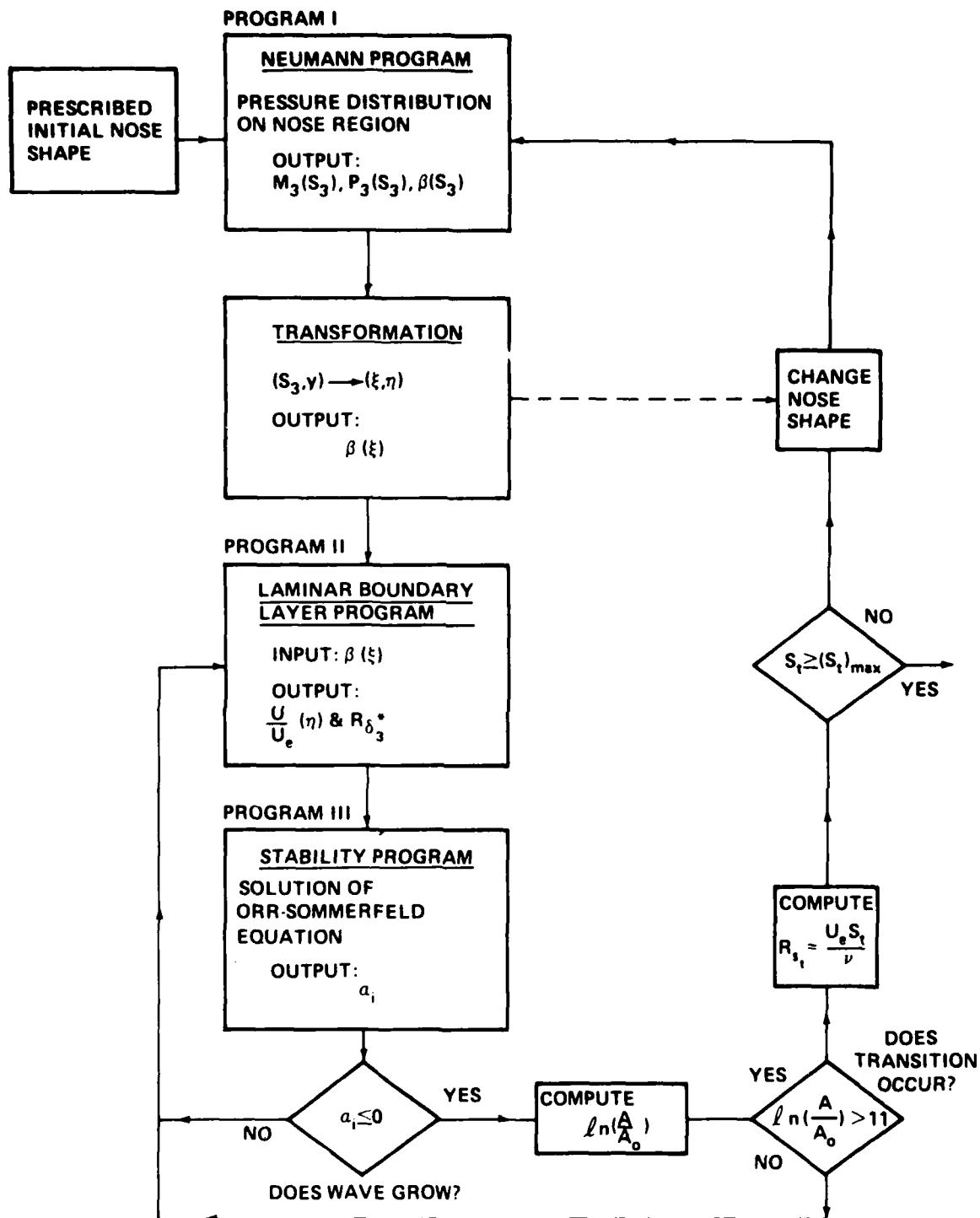
4

Figure 1 - Schematic Diagram of the Computational Algorithm
for the Design of a Nose Shape

are computed. From these results one must numerically evaluate M_3 given by equation (A5) as

$$M_3(s_3) = \frac{2s_3}{U_e} \frac{dU_e}{ds_3}$$

where

$$s_3 = \int_0^x \sqrt{1 + (\bar{r}_o')^2} \; dx$$

and s_3 is the distance along the body surface, $r_o(x)$ the radius of the body, and x is the axial distance measured from the nose of the body. In the vicinity of the stagnation point of a blunt body $\frac{U_e}{U_\infty} \propto s_3^m$, hence $\lim_{s_3 \to 0} (M_3) = 2m$. For the axisymmetric stagnation flow on a disk, $m = 1$, hence $\lim_{s_3 \to 0} M_3 = 2.0$. This value is used in all the computer studies. In general $2.0 \geq M_3 \geq 0$ and decreases with increasing s_3 in the favorable pressure gradient region.

B. Mangler Transformation into Two-Dimensional Coordinates

The axisymmetric coordinates (s_3, y_3) and the pressure gradient parameter M_3 are transformed into the equivalent two-dimensional similarity coordinates (ξ, η)* and pressure gradient parameter β through the equations (A2), (A3), and (A4) given as

$$\xi = \mu_e^2 \bar{U}_e R_D^2 \bar{r}_o^2 \frac{\bar{s}_3}{2P}$$

$$\eta = \sqrt{\frac{R_D \bar{U}_e P_3^2}{\bar{s}_3}} \; \bar{y}_3$$

$$\beta \, \xi = \frac{M_3}{2P_3^2(s_3)}$$

where $\bar{s}_3 = s_3/D$, $\bar{y}_3 = y_3/D$, $\bar{r}_o = r_o/D$, $\bar{U}_e = U_e/U_\infty$

---

*These are called the Mangler-Levy-Lees transformations, see Appendix A.

$$P_3^2 = \frac{\overline{s}_3 \overline{U}_e \overline{r}_o^2}{2 \int_o^{\overline{s}} {}^3 \overline{U}_e \overline{r}_o^2 ds_3} \quad .$$

The local value of β along the nose surface is the single most important external flow characteristic governing the laminar boundary layer properties and consequently, affecting the location of transition. Therefore, some comments are in order regarding the magnitude of this function in the favorable pressure gradient region downstream of the nose stagnation point. Again, assume $\frac{U_e}{U_\infty} \propto s_3^m$ and $r_o \propto s_3^p$ for the stagnation region on the axiymmetric body, then $\lim_{s_3 \to 0} (M_3) = 2m$ and $\lim_{s_3 \to 0} (2P_3^2) = 2p+m+1$ hence, $\beta(0) = \frac{2m}{2p+m+1}$. For the disk stagnation flow, $m = 1$ and $p = 1$, therefore $\beta(0) = 0.5$ and this value is used as the starting value for the computer solutions. In general, the range of values in the favorable pressure gradient region downstream of the nose are

$$2.0 \geq M_3(s_3) \geq 0 \qquad 2 \geq P_3^2(s_3) > \frac{1}{\sqrt{2}}$$

and

$$\boxed{0.5 \geq \beta(\xi) > 0.} \quad *$$

C. Two-Dimensional Laminar Boundary Layer Computations

The two-dimensional laminar boundary equation in the transformed coordinates is given as[4],

$$f''' + f'' + \beta[1-(f')^2] = 2\xi[f' \frac{\partial f'}{\partial \xi} - f'' \frac{\partial f}{\partial \xi}]$$

---

*It has been brought to our attention by Dr. von Kerczek that $\beta > 1$ can occur on flat faced bodies of revolution downstream of the stagnation point.

where $\dfrac{u}{U_e} = f'(\eta)$ and $\beta = $ function (M_3, P_3, ξ).

This equation is numerically solved for the velocity profile $\dfrac{u}{U_e}$ using the Cebeci-Smith method[4]. The displacement thickness δ^*_3 along the body surface is then computed through the equations (A8) and (A9)

$$\frac{R_{\delta^*_3}}{\sqrt{R_D}} = \sqrt{\frac{\overline{s}_3 \overline{U}_e}{P_3^2}} \quad \delta^*(\beta, \xi)$$

$$\frac{\delta^*_3}{D} = \sqrt{\frac{\overline{s}_3}{R_D \overline{U}_e P_3^2}} \quad \delta^*(\beta, \xi)$$

where

$$R_{\delta^*_3} = \frac{U_e \delta^*_3}{\nu} \quad , \quad R_D = \frac{U_\infty D}{\nu}$$

and

$$\delta^*(\beta, \xi) \equiv \int_0^\infty (1 - f') \, d\eta.$$

From this equation, it is seen that the body Reynolds number R_D has a direct effect on the displacement thickness δ^*_3 along with the value of β which enters through the computations of $\delta^*(\beta, \xi)$.

D. Orr-Sommerfeld Stability Computations

Using the velocity profile $\dfrac{u}{U_e}$ and the displacement thickness δ^*_3 in the axisymmetric coordinates (s_3, y_3), the Orr-Sommerfeld equation is solved numerically at each point along the body surface s_3 for selected frequencies of the disturbance waves. When one or more of these disturbance waves are found to grow $(\alpha_i < 0)$, then the amplification rate

8

$\ln(\frac{A}{A_o})$ is computed for each of these growing waves until at least one wave is found to supposedly erupt into a turbulent burst ($\ln \frac{A}{A_o} \approx 9\text{-}11$). This location is then defined as the location of transition S_t where $S_t =$ funct (shape, R_D).

The solution of this equation is a computational task of order of magnitude greater than the three other tasks. A major research effort is being pursued in developing more efficient algorithms that will reduce the computer execution time. The recent work by Von Kerczek[5] indicates that this task can be performed within reasonable execution times and cost.

Extensive numerical solutions to these equations have been obtained for a wide class of laminar velocity profiles referred to as similar flows. These are the cases when β = constant and $f = f(\eta)$ and includes conical shape noses[6] of half angle ϕ. These results clearly show the strong dependence of the location of instability on the values of β. More specifically, these results, to a rough approximation, give

Similar Flows[7]		Conical Similar Flows[7]	
β	$(R_{\delta*})_{crit}$	β	ϕ(cone half angle)
1.0	12,490	.500	90.0°
0.8	10,920	.421	81.6°
0.6	8,890	.333	71.3°
0.4	6,230	.210	58.2°
0.2	2,830	.125	40.3°
0.0	520	.064	27.7°
		.033	19.0°
		0	0°

---

[5] Von Kerczek, C., Private Communication.

[6] Evans, H.L., "Laminar Boundary-Layer Theory," Addison-Wesley Publishing Co., London, p.121, p.70 (1968).

[7] White, F.M., "Viscous Fluid Flow," McGraw-Hill, New York, p. 341, p. 405 (1974).

2.0 DISTINCT FEATURES OF AXISYMMETRIC FLOWS

2.1 DISTINCTION BETWEEN TWO-DIMENSIONAL AND AXISYMMETRIC FLOWS

A clear distinction should be made between the axisymmetric coordinates (s_3, y_3) where s_3 is the distance along the nose surface and y_3 is normal to the surface, and an equivalent two-dimensional system (s_2, y_2) such as that along a flat plate. Figure 2 summarizes the transformations and boundary layer characteristics for each of these cases.

The two systems are considered equivalent if, after the transformation, the transformed variables ξ, η are equivalent and $\beta_2 = \beta_3$. In order to make a comparison between the two-dimensional and axisymmetric system, two cases can be equated:

CASE I - Equivalent Downstream Distance

Given: $U_{e_3}(s_3)$ and $r_o(s_3)$

Assume: $s_3 = s_2$

Then, the two flows are equivalent when

$$y_2 = \bar{r}_o y_3 \qquad\qquad U_{e_2}(s_2) = \bar{r}_o^2 \, U_{e_3}(s_3).$$

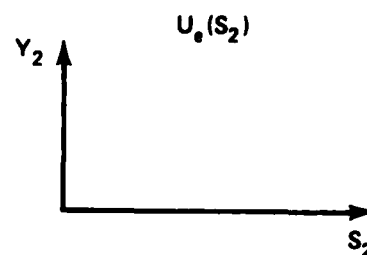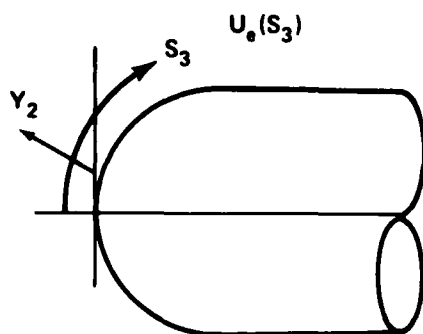CASE II - Equivalent Pressure Gradient in External Flow

Given: $U_{e_3}(s_3)$ and $r_o(s_3)$

Assume: $U_{e_2}(s_2) = U_{e_3}(s_3)$ or $M_3 = M_2$

Then, the two flows are equivalent when

$$y_2 = \bar{r}_o \, y_3 \qquad\qquad s_2 = \int_o^{s_3} \bar{r}_o^2 \, ds_3 \, .$$

10

BASIC ASSUMPTIONS: $S = S_2 = S_3$ AND $U_{e_2}(S) = U_{e_3}(S)$

AXISYMMETRIC FLOW	TWO-DIMENSIONAL FLOW

THEN $\quad M = M_3 = \dfrac{2S_3}{U_e} \dfrac{dU_e}{dS_3}$

THEN $\quad M = M_2 = \dfrac{2S_2}{U_e} \dfrac{dU_e}{dS_2}$

$$2P_3^2 = \frac{\overline{S}_3\, \overline{U}_e\, \overline{r}_0^2}{\displaystyle\int_0^{S_3} \overline{U}_e\, \overline{r}_0^2\, ds_3}$$

$$2P_2^2 = \frac{\overline{S}_2\, \overline{U}_e}{\displaystyle\int_0^{S_2} \overline{U}_e\, ds_2}$$

$$\beta_3 = \frac{1}{2P_3^2}\, M$$

$$\beta_2 = \frac{1}{2P_2^2}\, M$$

$$\sqrt{2} \geqslant P_3 > \frac{1}{\sqrt{2}}$$

$$1 \geqslant P_2 > \frac{1}{\sqrt{2}} = .707$$

$$0.5 \geqslant \beta_3 > 0$$

$$1.0 \geqslant \beta_2 > 0$$

$$\frac{R_{\delta_3^*}}{\sqrt{\overline{R}_{s_3}}} = \frac{1}{P_3(s)}\, \delta^*(\beta_3, \xi_3)$$

$$\frac{R_{\delta_2^*}}{\sqrt{\overline{R}_s}} = \frac{1}{P_2(s)}\, \delta^*(\beta_2, \xi_2)$$

$$\frac{\delta_3^*}{S_3}\sqrt{R_{s_3}} = \frac{R_{\delta_3^*}}{\sqrt{R_{s_3}}}$$

$$\frac{\delta_2^*}{S_2}\sqrt{R_{s_3}} = \frac{R_{\delta_2^*}}{\sqrt{R_{s_2}}}$$

Figure 2 - Comparison of Two-Dimensional and Axisymmetric
Boundary-Layer Properties

It is erroneous to make a direct comparison of the axisymmetric flow field with those of a two-dimensional system in which one equates both the distance downstream along a flat plate with the axisymmetric surface distance ($s_2 = s_3$) and assumes identical external pressure gradients ($M_2 = M_3$). The values of β used for the computation in the transformed coordinates (ξ, η) will be different and thus the computed boundary layer characteristics are not identical. By examining the equations given in Figure 2, one can show that in a favorable pressure gradient region near the nose or leading edge

two-dimensional flow   axisymmetric flow

$$1 \geq P_2 \geq \frac{1}{\sqrt{2}} \qquad\qquad \sqrt{2} \geq P_3 \geq \frac{1}{\sqrt{2}}$$

$$1.0 \geq \beta_2 \geq 0 \qquad\qquad 0.5 \geq \beta_2 \geq 0$$

Consequently, the pressure gradient parameter β_2 on the equivalent flat plate will be higher by a factor of 2 from the true axisymmetric pressure gradient β_3 despite the fact that both systems have the same external flow fields.

It can also be shown that the displacement thickness ratio between the actual δ^*_3 and the equivalent two-dimensional δ^*_2 will be

$$\frac{\delta^*_3}{\delta^*_2} = \frac{P_2(s_2)}{P_3(s_3)} \frac{\delta^*(\beta_2,\xi_2)}{\delta^*(\beta_3,\xi_3)} \approx \frac{1}{\sqrt{2}} \frac{\delta^*(\beta_2,\xi_2)}{\delta^*(\beta_3,\xi_3)}$$

where $\beta_2 > \beta_3$ and $\xi_2 > \xi_3$.

Similarly, solutions of the boundary layer equations, $\delta^*(\beta)$, decrease slightly with increasing values of β, as shown below[7],

β	Similarity $\delta*(\beta)$	Elliptical Forebodies					
		t=1.00		t=.500		t=.250	
		$\delta*(\beta,\xi)$	P_3^2	$\delta*(\beta,\xi)$	P_3^2	$\delta*(\beta,\xi)$	P_3^2
1.00	.648	-	-	-	-	-	-
.50	.804	.804	2.00	.804	2.00	.804	2.00
.40	.852	.836	1.73	.842	1.82	-	-
.30	.911	.871	1.58	.889	1.66	-	-
.20	.984	.911	1.47	.949	1.46	.945	~1.54
.10	1.080	.958	1.39	1.020	1.23	1.040	~1.30
.0	1.217	.996	1.33	1.113	1.06	1.172	~1.00

"t" in the above set of values, is the ratio of the minor-to-major axis

Therefore $\qquad \delta*(\beta_2) < \delta*(\beta_3)$ or $\dfrac{\delta*(\beta_2)}{\delta*(\beta_3)} \doteq 0.82.$

By examining various numerical examples, one obtains the approximation that

$$\delta*_3 \approx 0.86 \, \delta*_2$$

and leads one to speculate that in general, the displacement thickness along an axisymmetric body would be slightly thinner than the equivalent displacement thickness along a flat plate with the identical pressure distribution.

In summary, two generalized remarks can be made*:

i)   The pressure gradient imposed by the external flow on an axisymmetric body is weaker than the equivalent pressure gradient imposed on a two-dimensional flat plate.

---

*Similar conclusions have been expressed by Kaups on page 10 of Douglas Report No. MDC J6530 (April 1974).

13

ii) The _displacement thickness_ on the axisymmetric body, δ_3^* , is _thinner_ than that which would exist on the flat plate with an equivalent pressure gradient.

The fact that the boundary layer characteristics on an axisymmetric body are different than those on a flat plate requires one to interpret this distinction from the standpoint of their effect on transition. By comparing the location of transition on an axisymmetric body with that of a flat plat with identical pressure distribution, the weaker pressure gradient, in terms of β, is an adverse effect to enhancing a stable flow while the thinner boundary layer is a favorable effect[8].

2.2 LOCALIZED FLOW PROPERTIES GOVERNING TRANSITION

In the discussion on the stability prediction method, it has been emphasized that the local values of the pressure gradient parameter β have a strong influence on the location of transition. Specifically, that transition is delayed by a strong favorable pressure gradient (β as large as possible). The values of β are inherently related to the geometrical shape of the body and, as previously discussed, require different interpretations for two-dimensional and axisymmetric flows.

Let us try to see, more specifically, how the magnitude of β affects the onset of transition. Consider a favorable pressure gradient $0.5 \geq \beta(s_3) \geq 0$ representing the region downstream of the stagnation point. One can present a somewhat simplified and qualitative interpretation of the transition process by arguing that the instability of a disturbance wave will occur when the local displacement thickness $R_{\delta_3^*}(s_3)$,

---

[8]Kaups, K., "Transition Prediction on Bodies of Revolution," Report No. MDC J6530, Douglas Aircraft Co., Long Beach, California (Apr 1974).

14

computed at each downstream position, exceeds a certain critical value $(R_{\delta*})_{crit}$. Some justification for using the dimensionless displacement thickness as a measure of the stability threshold are presented by Lighthill[9] in which $R_{\delta*}$ is interpreted as a ratio of the convection rate to diffusion rate of a disturbance in the vorticity field. Alternatively, one could use the dimensionless momentum thickness R_θ since this appears to be the fundamental characteristic proposed by Granville in Reference 2.

The displacement thickness $R_{\delta*_3} = \left(\dfrac{U_e \delta*_3}{\nu}\right)$ increases along the downstream distance because of the growth of the boundary layer. The particular rate of the growth depends on the local values of the pressure gradient parameter β, and the body Reynolds number R_D. On the other hand, the critical Reynolds number $(R_{\delta*})_{crit}$ has an extremely large value at the stagnation point but decreases, rather drastically, along the downstream distance because of the decreasing β. When the increasing value of $R_{\delta*_3}$ equals the decreasing critical value $(R_{\delta*})_{crit}$, transition will occur. Figure 3 schematically illustrates this condition for three arbitrary body shapes. The key to delaying transition is then two-fold:

i) Extended Favorable Pressure Gradient Region

The local pressure gradient parameter β should be as large as possible over an extended region in order for a high critical Reynolds number or $(R_{\delta*})_{crit} =$ funct (β) should be large.

ii) Thin Boundary Layer During Downstream Development

The boundary layer growth should be as thin as possible during its downstream development, or $R_{\delta*_3} =$ function (P_3, β, R_D) should be

_____

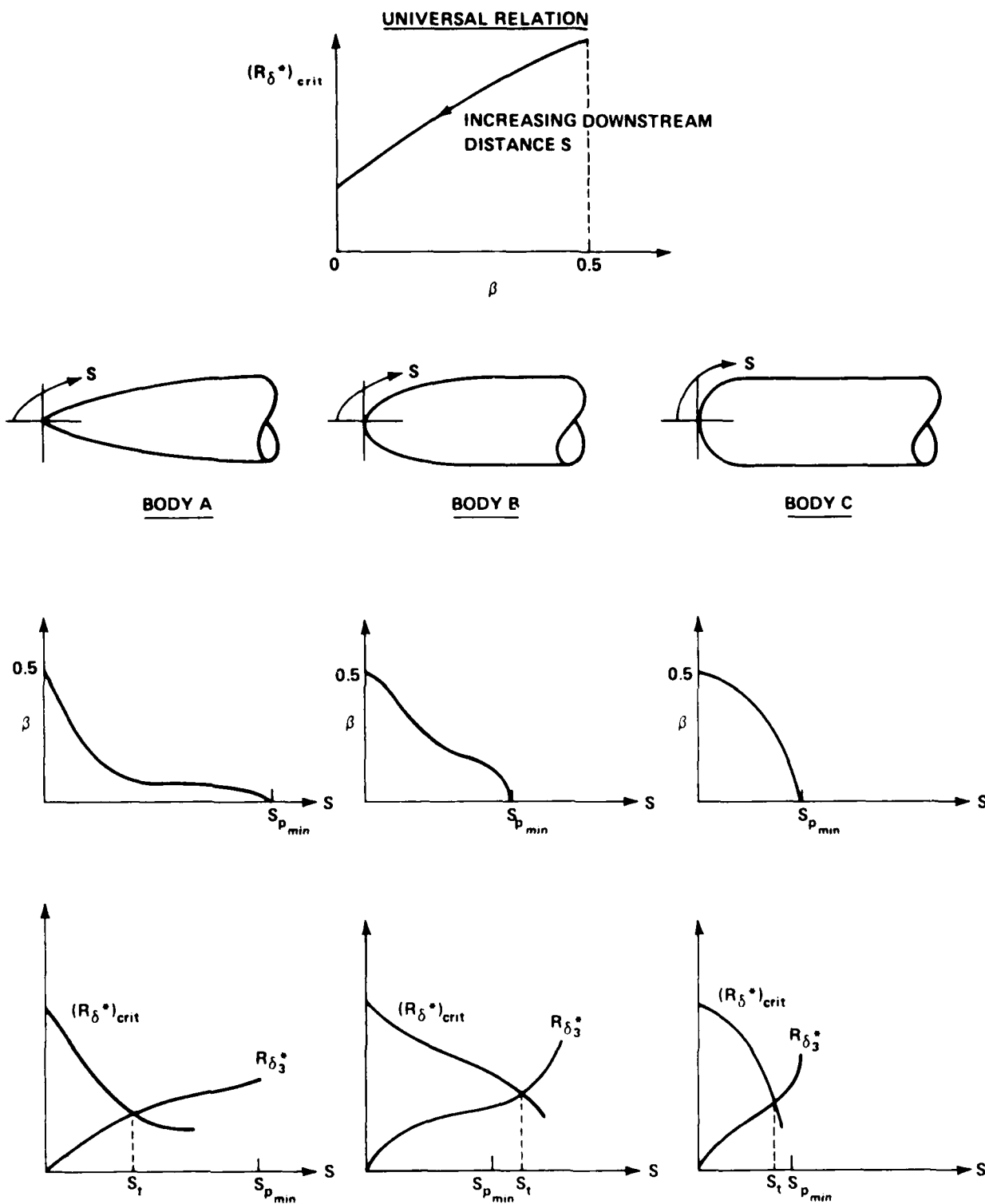[9]Rosenhead, L., "Laminar Boundary Layers," Clarendon Press, Oxford, England, p. 88-90 (1963).

15

Figure 3 – Schematic Diagrams Illustrating the Effects of
Nose Shapes on the Location of Transition

16

small. Note that equation (A9) gives

$$R_{\delta_3^*} = \sqrt{\frac{\overline{s}_3 \overline{U}_e R_D}{P_3^2}} \qquad \delta^*(\beta,\xi) \approx \frac{\delta^*(\beta,\xi)}{\sqrt{2}} \ \sqrt{\overline{s}_3 \overline{U}_e R_D}$$

where

$$\frac{\delta^*(.5,0)}{\sqrt{2}} \approx \frac{.804}{1.414} \approx .568.$$

Both of these aspects are enhanced by a $\beta(S_3)$ function which decreases at the slowest possible rate from its maximum value at the stagnation point.

It is important to note that the rate of growth of the boundary layer thickness is strongly influenced by the body Reynolds number $R_D = \dfrac{U_\infty D}{\nu}$, more so than by the magnitude of β. Therefore, despite the advantages of the favorable pressure gradient in delaying transition past the $(C_p)_{min}$ location, transition can still move forward and occur within the favorable pressure gradient region at very high Reynolds number R_D. This is illustrated in Figure 4 for body B of previous figure.

A comparative evaluation of several body shapes can be made by examining the behavior of the β curves downstream of the stagnation point for each of these shapes. These results can be obtained from the potential flow computation (Program I). Figure 5 illustrates these β computations for the standard ellipsoidal forebodies obtained from the Neumann Program. Imposed on these figures is the β curve for an "idealized" shape body possessing the property of a large value of β and consequently a large value of $(R_{\delta^*})_{crit}$ downstream of the stagnation point.

The growth rate of the boundary layer downstream of the stagnation point is also an important feature in evaluating several body shapes. The laminar boundary layer computations for each of the body shapes are required (Program II). However, as one would expect, the shape of these curves downstream of the stagnation point are initially quite similar
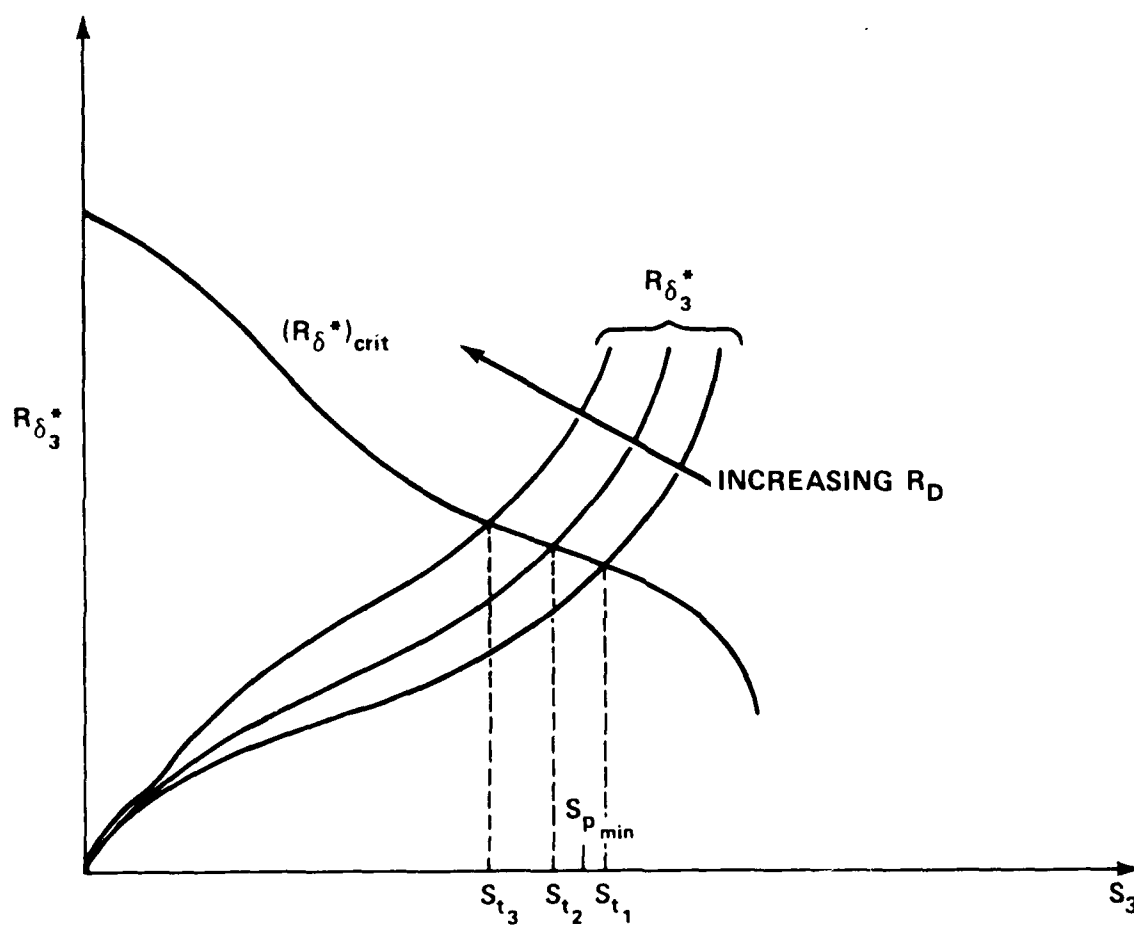
17

Figure 4 – Schematic Diagram Illustrationg the Effect of Body
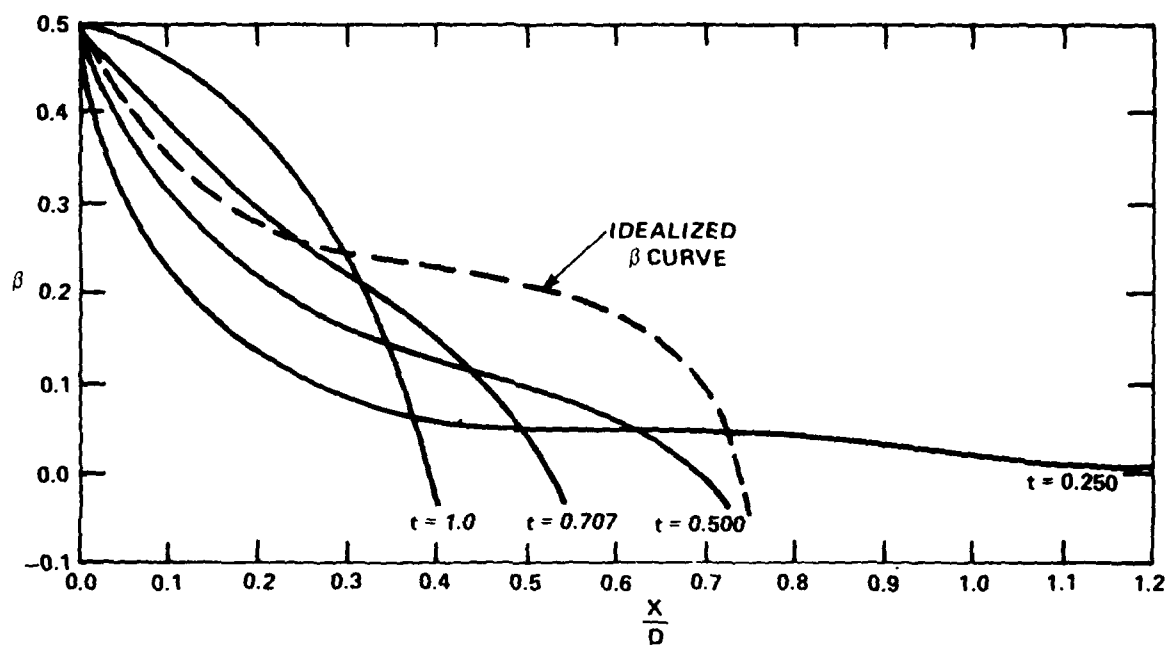Reynolds Number R_D on the Location of Transition

Figure 5 – Pressure Gradient Parameter β for Family
of Ellipsoidal Forebodies

until $\beta \rightarrow 0$ for each of the respective shapes. Figure 6 illustrates these computations for ellipsoidal nose shapes at fixed R_D.

3.0 EFFECTS OF GEOMETRIC SHAPE ON TRANSITION

3.1 COMPARISON OF VARIOUS SHAPES AT FIXED R_D

As previously stated, the first task in any evaluation of the location of transition on an axisymmetric nose is to compute the potential flow or pressure distribution around the body surface. The relationship between the geometrical shape of an axisymmetric body and the shape of the pressure distribution curve (C_p versus $\frac{X}{D}$) or the freestream velocity curve ($\frac{U_e}{U_\infty}$ versus $\frac{X}{D}$) has been extensively studied. The two most characteristic features are the magnitude and location of $(C_p)_{min}$ or alternately, the magnitude and location of $(\frac{U_e}{U_\infty})_{max}$ where $C_p = 1 - (\frac{U_e}{U_\infty})^2$. Figure 7 illustrates the $\frac{U_e}{U_\infty}$ curves for a family of elliptic noses. The streamwise body surface location of $(C_p)_{min}$ for each of the bodies, denoted earlier as $S_{p_{min}}$, is easily seen in Figure 7 and shows that the more blunt the body shape, the less the extent of the favorable pressure gradient region.

The M_3 curve can, to a resonably good approximation, be interpreted as the β curve. The local value of M_3 or β at each point along the body surface can be correlated with the slope of the body shape obtained by drawing a tangent line at the body surface. A large slope gives a large value of β. This conjecture is based on examining conical similar flows which give constant values of β for conical half angles ϕ, these values of β versus ϕ are tabulated on page 9 of this report. In fact, a conical shape with ϕ large downstream of a spherical nose cap would ideally represent a good shape since $\beta > 0$ over the downstream distance. However,
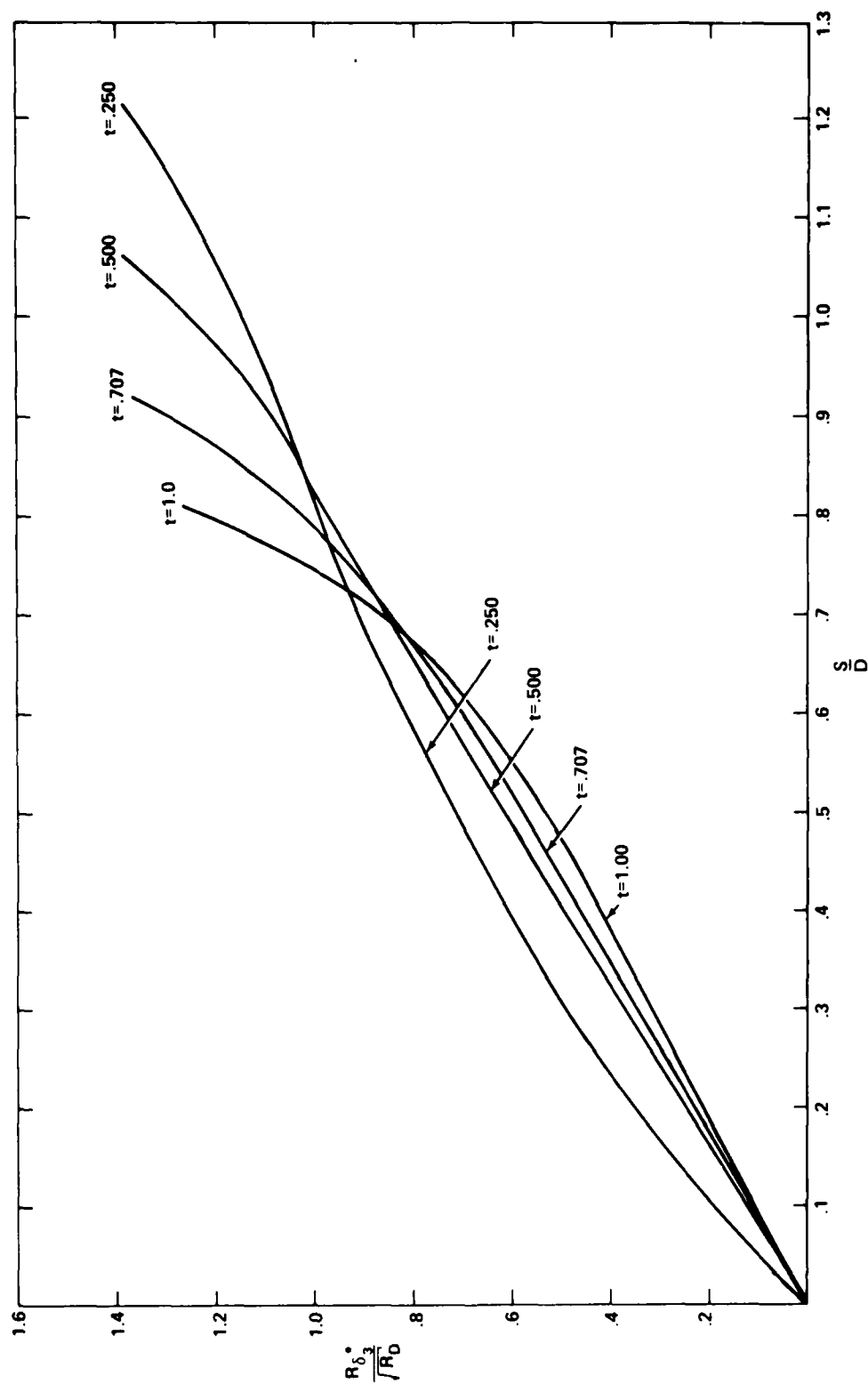
Figure 6 – Dimensionless Displacement Thickness for Ellipsoidal
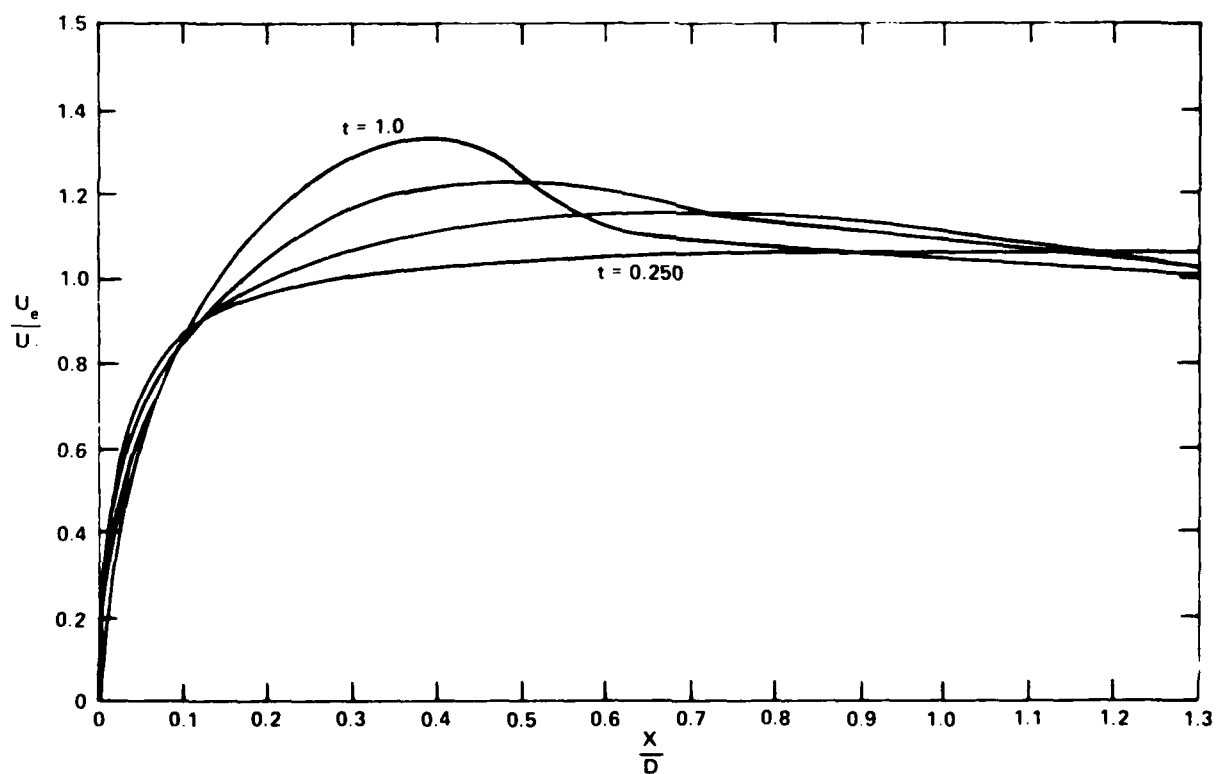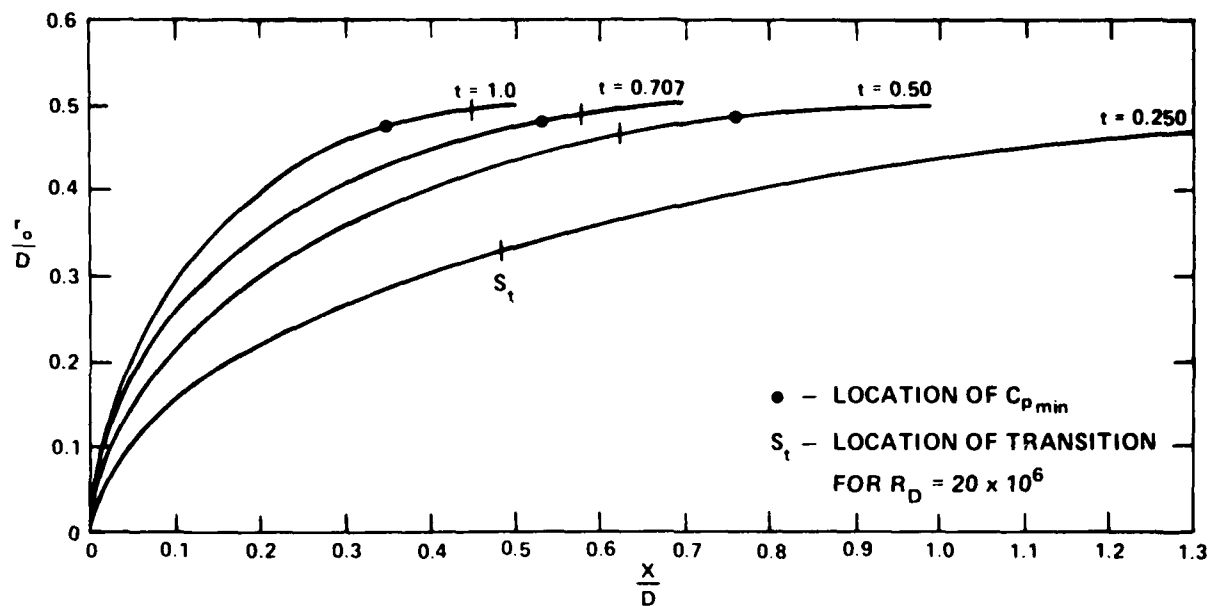Forebodies, t=1.0, 0.707, 0.50, 0.25

Figure 7 - Velocity Distribution for Ellipsoidal Forebodies,
t=1.0, 0.707, 0.50, 0.25

in order to realistically attach this conical shape smoothly to a cylindrical body of prescribed diameter, the conical surface distance would be quite limited. Therefore a large pressure gradient would exist but would not extend far enough downstream.

As previously discussed, the effects of body shape on the growth of the boundary layer thickness for a fixed R_D does not appear to be a significant factor except in the vicinity of $(C_p)_{min}$, where an abrupt increase exists for each of the respective shapes.

As emphasized earlier, a large positive value of β is desirable downstream of the stagnation point for as large a downstream distance as possible. A tradeoff clearly becomes evident between a <u>large favorable pressure gradient</u> (β large) and an <u>extended favorable pressure gradient region</u> ($S_{P_{min}}$ large). A good design of a nose shape is one that can optimize these conditions.

The location of the transition point S_t on each body shape is shown in Figure 7 for an $R_D = 20 \times 10^6$. These results were obtained from those reported by Kaups (MDC J6530, April 1974) in which the Smith-Gamberoni prediction method was used. These results confirm the arguments just presented. For the elliptic noses shown in Figure 7, the nose with an aspect ratio of $t = .50$ has transition occurring farthest downstream. Inspection of the β curves would indicate that $t = .500$ and $t = .707$ have the best shapes among the four candidates. In summarizing the conclusions on the effect of body shape on transition, one should inspect the $(C_p$ versus $\frac{X}{D})$, $(\beta$ versus $\frac{X}{D})$, and $(\frac{R_{\delta^3}}{\sqrt{R_D}}$ versus $\frac{S}{D})$ curves for several shape noses and conclude that the "best shape" is the one with the following attributes:

i) The location of $(C_p)_{min}$ should be as far downstream of the nose as possible. ($\beta > 0$ exists over an extended region).

ii) The values of β should be as large as possible in the upstream vicinity of $S_{p_{min}}$. (β large positive number).

iii) The value of $(\frac{U_e}{U_\infty})_{max}$ should be as small as possible.

iv) The value of $R_{\delta^*_3}$ should be as small as possible in the upstream vicinity of $S_{p_{min}}$.

v) The value of the roughness height should be less than 20 per cent of δ^*_3 in the upstream vicinity of $S_{p_{min}}$.

The conflicting conditions (i) and (ii) are a direct consequence of the fact that stability is delayed by a favorable pressure gradient. The third conjecture is a result of the fact that achieving $(R_{S_t})_{max} = (\frac{U_e S_t}{\nu})_{max}$ does not necessarily assure you that $(S_t)_{max}$ has been achieved since the local velocity $U_e(s)$ is also increasing in the favorable pressure gradient region. Furthermore, the boundary layer growth rate increases with increasing $\frac{U_e}{U_\infty}$. Thus, condition (iii) also introduces a conflict with the criteria suggested under conditions (i) and (ii). Therefore, an optimum condition must exist on choosing the shape with rather unique pressure distribution features.

Conditions (iv) and (v) are based on examining the results from the boundary layer computations and are of secondary importance in assessing a good shape. Condition (v) is only a reminder that with decreasing δ^*_3, desirable for delaying transition, one is more likely to trip transition by means of a surface proturberance.

3.2 EFFECT OF HIGH REYNOLDS NUMBER ON TRANSITION

In designing the best possible nose shape for high Reynolds number operation ($R_D > 30 \times 10^6$) it is the authors' conjecture that the best that

one can hope for is that transition will occur at or slightly downstream of the location of the minimum pressure $(C_p)_{min}$ or that

$$S_t \approx S_{P_{min}}.$$

For these high Reynolds numbers, the dimensionless boundary layer rate of growth, given by equation (A 9)

$$R_{\delta_3^*} \approx \frac{1}{\sqrt{2}} \; \delta^*(\beta,\xi) \; \sqrt{\frac{s_3}{D} \cdot \frac{U_e}{U_\infty} \cdot R_D}$$

increases as $\sqrt{R_D}$ and this is illustrated schematically in Figure 4. It is clear that with increasing body Reynolds number, transition will continuously move upstream and eventually occur within the favorable pressure gradient region. This is confirmed by the results obtained by Kaups[8] and illustrated in Figure 8 for elliptical shape noses. At Reynolds number above $R_D = 30 \times 10^6$, transition moves upstream of the $S_{P_{min}}$ location for most the bodies shown in Figure 8. Therefore, a large value of β upstream of the $S_{P_{min}}$ location, will slow down the upstream movement of the transition point S_t with increasing speed or Reynolds number R_D.

Furthermore, the "best shape" for transition postponement at a low Reynolds number might not be the best choice at higher Reynolds number. Examining Figure 8 shows that the elliptical nose with an aspect ratio of $t = .500$ delays transition the farthest downstream at $R_D = 10 \times 10^6$ while the more blunt nose body with an aspect ratio of $t = .707$ delays transition the farthest at a body Reynolds number of $R_D = 50 \times 10^6$.
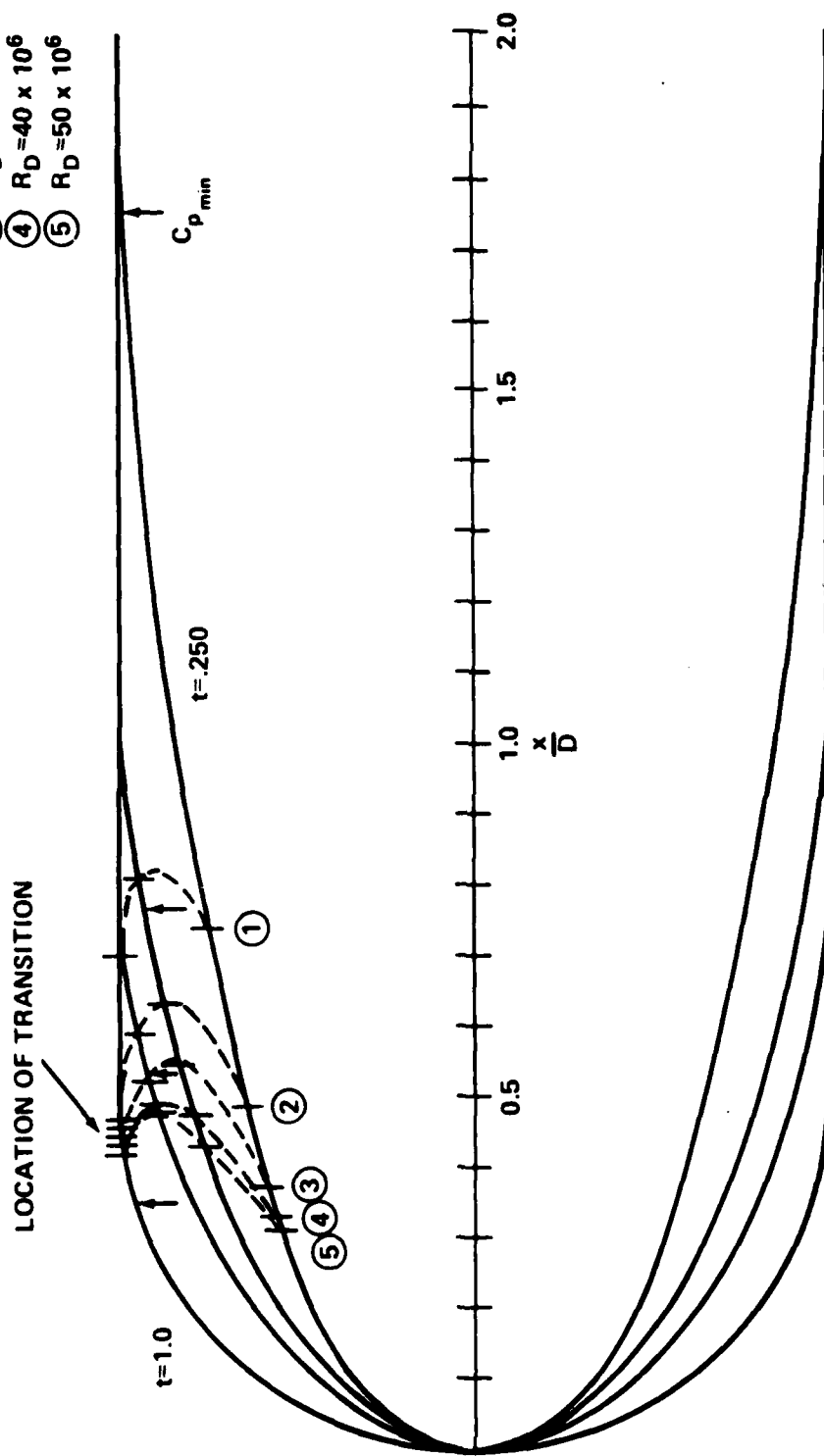
Figure 8 — Effects of Nose Shape and Reynolds Number on the Location of Transition

It should be realized that with an increasing R_D, the thickness of the boundary layer actually decreases. This can be deduced from equation (A8) which gives

$$\frac{\delta^*_3}{D} = \sqrt{\frac{\dfrac{s_3}{D}}{R_D \dfrac{U_e}{U_\infty} P_3^2}} \;\; \delta^*(\beta,\xi) \approx \frac{1}{\sqrt{2}} \sqrt{\frac{\dfrac{s_3}{D}}{\dfrac{U_e}{U_\infty} \cdot R_D}} \;\; \delta^*(\beta,\xi)$$

where

$$\frac{\delta^*(0.5,0)}{\sqrt{2}} = .568 \quad \text{and} \quad 1.2 \geq \delta^*(\beta,\xi) \geq .804$$

Thus, the possibility of roughness tripping the laminar boundary layer increases significantly at high Reynolds numbers.

The remarks made on the effects of high Reynolds number on transition should be interpreted as being somewhat speculative. Experimental data is seriously lacking in both understanding the complex transition process under these conditions, and confirming the validity of the stability prediction method at these high Reynolds numbers. Even the most basic types of laboratory experiment are not usually possible in the range of Reynolds number under consideration. Secondary effects such as surface roughness can play a governing role on the transition process at these conditions. Experimental tests on large axisymmetric bodies are required in order to shed light and give further direction to the factors governing transition under these extreme conditions.

4.0 SUMMARY AND CONCLUSIONS

A study was made to examine and gain insight into the inherent features and characteristics of the laminar boundary layer on axisymmetric

27

bodies that are used as a basis for the Smith-Gamberoni method of pre-
dictions. The ability of the method to accurately predict, for a given
body shape and prescribed body Reynolds number R_D, the location of
transition can only be attested by comparing the predictions with experi-
mentally obtained results such as those obtained by DTNSRDC. However,
accepting the condition that this method reflects the current state-of-the-
art for prediction techniques, an effort was made to examine carefully
those potential flow and laminar boundary layer characteristics of the
viscous flow region that are used as input for the complex stability
computations, and to find a correlation between certain geometrical and
hydrodynamic characteristics of a given body shape, and to ascertain the
ability of that shape in delaying transition.

For purposes of explanation, the transition process is envisioned
as the condition under which the downstream growth of the boundary layer,
denoted by $R_{\delta *}$, is such that it exceeds a critical value $(R_{\delta *})_{crit}$ and
that the sophisticated stability computation program is essentially per-
forming this computation as rigorously and accurately as possible. Based
on this interpretation, the key to delaying transition is to maintain
as thin a boundary layer as realistically possible and provide an
external flow environment with a strong favorable pressure gradient.

It is suggested that a comparative evaluation of various shapes
be made without extensive boundary layer computations or stability com-
putations but by simply comparing the shapes of the pressure gradient
parameter β curves from the stagnation point downstream until the $C_{P_{min}}$
location is reached. It is concluded, with a certain degree of con-
jecture, that the best shape for delaying transition is correlated with

28

shape of the β curve. It should be emphasized that one can compute the β curves for each body directly from the potential flow computations. The question of obtaining the "optimum design" of a nose shape is not straightforward but the inherent boundary layer characteristics most favorable in delaying transition are discussed and some examples of geometrical shapes for which stability computations have been performed are presented to show the attributes of a good design. These examples give some direction to future work in obtaining optimal designs.

An important area for immediate assessment is the effect of high body Reynolds number on the transition process. This has been addressed with a certain degree of speculation since experimental data is seriously lacking in either shedding light on the transition process or in confirming the validity of the stability prediction methods at these Reynolds numbers.

ACKNOWLEDGEMENT

REFERENCES

1. DeMetz, F.C. and M.J. Casarella, "An Experimental Study of the Intermittent Properties of the Boundary Layer Pressure Field During Transition on a Flat Plate," NSRDC Report 4140 (November 1973).

2. Granville, P.S., "The Calculation of the Viscous Drag of Bodies of Revolution," DTMB Report No. 849 (July 1953).

3. Niedzwecki, J., "Laminar and Turbulent Incompressible Boundary Layers on Bodies of Revolution in Axial Flow," Doctoral Dissertation, Catholic University of America, Dept. of Mechanical Engineering (Feb 1977).

4. Cebeci, T. and A.M.O. Smith, "Analysis of Turbulent Boundary Layers," Academic Press, New York (1974).

5. Von Kerczek, C., Private Communication.

6. Evans, H.L., "Laminar Boundary-Layer Theory," Addison-Wesley Publishing Co., London, p. 121, p. 70 (1968).

7. White, F.M., "Viscous Fluid Flow," McGraw-Hill, New York, p. 341, p. 405 (1974).

8. Kaups, K., "Transition Prediction on Bodies of Revolution," Report No. MDC J6530, Douglas Aircraft Co., Long Beach, California (Apr 1974).

9. Rosenhead, L., "Laminar Boundary Layers," Clarendon Press, Oxford, England, p. 88-90 (1963).

APPENDIX A

Summary of the Transformations for Flat Plates and Axisymmetric Bodies

A.1 The Coordinate Transformations

A.1.1 The Cebeci-Smith Form

Flat Plate (k=0)   **Axisymmetric Body (k=1)**

$$d\xi = \rho\mu_e u_e dS_2 \qquad\qquad\qquad d\xi = \rho\mu_e u_e \bar{r}_o^2 \, dS_3$$

$$d\eta = \frac{\rho u_e}{\sqrt{2\xi}} \, dy_2 \qquad\qquad\qquad d\eta = \frac{\rho u_e}{\sqrt{2\xi}} \, \bar{r}_o \, dy_3$$

A.1.2 The Generalized Mangler Form

Flat Plate (k=0)   **Axisymmetric Body (k=1)**

$$d\xi = \mu_e^2 \bar{u}_e R_L \, d\bar{S}_2 \qquad\qquad d\xi = \mu_e^2 \bar{u}_e R_D \, \bar{r}_o^2 \, d\bar{S}_3 \qquad (A1)$$

$$d\eta = \frac{\mu_e \bar{u}_e}{\sqrt{2\xi}} R_L \, d\bar{y}_2 \qquad\qquad d\eta = \frac{\mu_e \bar{u}_e}{\sqrt{2\xi}} R_D \, \bar{r}_o \, d\bar{y}_3$$

<center>or</center>   <center>or</center>

$$\xi = \mu_e^2 \bar{u}_e R_L \frac{\bar{S}_2}{2P_2^2} \qquad\qquad \xi = \mu_e^2 \bar{u}_e R_D \, \bar{r}_o^2 \, \frac{\bar{S}_3}{2P_3^2} \qquad (A2)$$

$$\eta = \sqrt{\frac{R_L \bar{u}_e P_2^2}{\bar{S}_2}} \, \bar{y}_2 \qquad\qquad \eta = \sqrt{\frac{R_D \bar{u}_e P_3^2}{\bar{S}_3}} \, \bar{y}_3 \qquad (A3)$$

$$P_2^2 = \frac{\bar{S}_2 \bar{u}_e}{2 \int_o^{\bar{S}_2} \bar{u}_e \, dS} \qquad\qquad P_3^2 = \frac{\bar{S}_3 \bar{u}_e \bar{r}_o^2}{2 \int_o^{\bar{S}_3} \bar{u}_e \bar{r}_o^2 \, dS}$$

$$R_L = \frac{u_\infty L}{\nu} \qquad\qquad\qquad R_D = \frac{u_\infty D}{\nu}$$

$$\bar{S}_2 = \bar{x} \qquad\qquad\qquad\qquad L = D$$

Both cases have drawn upon the following definitions.

$$\overline{S}_{k+2} = \frac{S_{k+2}}{L} \qquad\qquad \overline{y}_{k+2} = \frac{y_{k+2}}{L}$$

$$\overline{x} = \frac{x}{L} \qquad\qquad \overline{r}_o = \frac{r_o}{D}$$

$$\overline{u}_e = \frac{u_e}{u_\infty} \qquad\qquad \nu = \frac{\mu}{\rho}$$

Note that for the flat plate case it can be shown that, as expected, ξ and η are independent of any length scale L.

A.2 The Pressure Gradient Parameter

Flat Plate (k=0)   Axisymmetric Body (k=1)

$$\beta = \frac{M_2}{2P_2^2} \qquad\qquad\qquad \beta = \frac{M_3}{2P_3^2} \qquad\text{(A4)}$$

$$M_2 = R_2 \frac{2\overline{x}}{\overline{u}_e} \frac{d\overline{u}_e}{d\overline{x}} \qquad\qquad M_3 = R_3 \frac{2\overline{x}}{\overline{u}_e} \frac{d\overline{u}_e}{d\overline{x}} \qquad\text{(A5)}$$

$$R_2 = 1 \qquad\qquad\qquad R_3 = \frac{\overline{S}_3}{\overline{x}\sqrt{1 + (\overline{r}_o')^2}} \qquad\text{(A6)}$$

$$\overline{r}_o' = \frac{d\overline{r}_o}{d\overline{x}}$$

$$P_2^2 = \frac{\overline{S}_2 \overline{u}_e}{2\displaystyle\int_0^{\overline{S}_2} \overline{u}_e\, dS} \qquad\qquad P_3^2 = \frac{\overline{S}_3 \overline{u}_e \overline{r}_o^2}{2\displaystyle\int_0^{\overline{S}_3} \overline{u}_e \overline{r}_o^{2k}\, dS} \qquad\text{(A7)}$$

A.3 Boundary Layer Properties

Flat Plate (k=0)   Axisymmetric Body (k=1)

$$\frac{\delta_2^*}{L} = \frac{M^+}{R_L \overline{u}_e}\; \delta^*(\beta,\xi) \qquad\qquad \frac{\delta_3^*}{D} = \frac{M^+}{R_D \overline{u}_e}\; \delta^*(\beta,\xi) \qquad\text{(A8)}$$

$$\frac{R_{\delta_2^*}}{\sqrt{R_L}} = \frac{M^+}{\sqrt{R_L}} \ \delta^*(\beta,\xi) \qquad\qquad \frac{R_{\delta_3^*}}{\sqrt{R_D}} = \frac{M^+}{\sqrt{R_D}} \ \delta^*(\beta,\xi) \qquad (A9)$$

$$\frac{\theta_2}{L} = \frac{M^+}{R_L \bar{u}_e} \ \theta(\beta,\xi) \qquad\qquad \frac{\theta_3}{D} = \frac{M^+}{R_D \bar{u}_e} \ \theta(\beta,\xi) \qquad (A10)$$

$$\frac{R_{\theta_2}}{\sqrt{R_L}} = \frac{M^+}{\sqrt{R_L}} \ \theta(\beta,\xi) \qquad\qquad \frac{R_{\theta_3}}{\sqrt{R_D}} = \frac{M^+}{\sqrt{R_D}} \ \theta(\beta,\xi) \qquad (A11)$$

$$H = \frac{\delta^*(\beta,\xi)}{\theta(\beta,\xi)} \qquad\qquad H = \frac{\delta^*(\beta,\xi)}{\theta(\beta,\xi)} \qquad (A12)$$

$$c_f = \frac{2}{M^+} \ f_w'' \qquad\qquad c_f = \frac{2}{M^+} \ f_w'' \qquad (A13)$$

$$M^+ = \sqrt{\frac{R_L \bar{S}_2 \bar{u}_e}{P_2^2}} \qquad\qquad M^+ = \sqrt{\frac{R_D \bar{S}_3 \bar{u}_e}{P_3^2}} \qquad (A14)$$

Both cases have drawn upon the following definitions,

$$\delta^*(\beta,\xi) = \int_0^\infty (1-f') \ d\eta \qquad\qquad \theta(\beta,\xi) = \int_0^\infty f'(1-f') \ d\eta$$

$$R_{\delta_{k+2}^*} \equiv \frac{u_e \delta_{k+2}^*}{\nu} \qquad\qquad R_{\theta_{k+2}} \equiv \frac{u_e \theta_{k+2}}{\nu}$$

A.4 Turbulent Flow Parameters

For both cases the following equations are utilized,

$$\bar{u}_\tau = \sqrt{\frac{c_f}{2}}$$

$$u^+ = \frac{u}{\bar{u}_\tau}$$

$$y^+ = M^+ \bar{u}_\tau \, \eta$$

where M^+ is defined in Section A.3.

INITIAL DISTRIBUTION

Copies		Copies	
1	Defense Advance Research Projects Agency	2	Aerospace Corp., Los Angeles, CA
	1 G.L. Donohue		1 J.W. Murdock
			1 T.D. Taylor
3	CHONR		
	1 Code 468, H.M. Fitzpatrick	1	DCW Industries, Inc.
	1 Code 438, R.D. Cooper		1 D.C. Wilcox
	1 Code 474, N. Perrone		
		1	Flow Research Inc.
3	NRL		Los Angeles, CA
	1 Dr. Hansen		1 C.L. Merkle
	1 O.M. Griffin		
	1 R.A. Skop	1	Jet Propulsion Lab., Pasadena, CA
			1 L.M. Mack
4	NAVSEA		
	1 SEA 0351, T.E. Peirce	3	McDonell Douglas Corp.
	1 SEA 037		1 A.M.O. Smith
	1 SEA 0372, A.R. Paladino		1 T. Cebeci
	1 PMS 395, J. Granet		1 K. Kaups
4	NOSC, San Diego	1	Physical Dynamics, Inc.
	1 Dr. A. Fabula		1 M.L. Finson
	1 Dr. J. Hoyt		
	1 Mr. H. Patrick	2	Physical Sciences Inc., Torrance, CA
	1 Mr. T.G. Lang		1 D.R.S. Ko
			1 M. Kosecoff
2	NUSC, Newport		
	1 Mr. B. Myers	4	Rand Corp., Santa Monica, CA
	1 Mr. D. Goodrich		1 C. Gazley
			1 J. Aroesty
1	NUSC, NLONLAB		1 E. Van Driest
	1 Dr. H. Schloemer		1 W. King
2	NAVSEC	4	Rockwell Intern. Autonetics Group
	1 SEC 6110		1 D.B. Moody
	1 SEC 6136		1 C. Jennings
			1 B. Carmichael
3	USNA		1 R. Scotti
	1 Dr. B. Johnson		
	1 Dr. S. Elder		
	1 Library		
1	National Bureau of Standards		
	1 P.S. Klebanoff		
1	Adv. Tech. Center Inc., Texas	1	Silencing Tech. Assoc.
	1 C.S. Wells		1 G. Franz

Copies		Copies	
2	Westinghouse Electric Corp. Annapolis, MD.	2	Virginia Polytechnic Inst. and State Univ.
	1 R.F. Mons		1 W.S. Saric
	1 R. Gulino		1 A.H. Nayfeh
1	Westinghouse Research Corp. Pittsburg, PA	1	Univ. of Rhode Island
	1 F.R. Goldschmied		1 F.M. White

CENTER DISTRIBUTION

3	Case Western University	1	15 Cummins
	1 Dr. E. Reshotko	1	1505 Crump
	1 H.L. Rogler	1	1522 Robinson
	1 A. Strazisar	1	154 Morgan
3	Univ. of California, Berkeley	1	1541 Granville
	1 P. Lieber	1	1552 McCarthy
	1 K.S. Wen	1	1552 Huang
	1 J.S. Marks	1	1552 Von Kerczek
		1	1552 Power
2	Univ. of California, Los Angeles	1	19 Sevik
	1 S.J. Barker	1	1901 Strasberg
	1 A.R. Wazzan	1	1902 Maidanik
		1	1903 Chertock
3	Catholic Univ of America	1	1905 Biancardi
	1 M. Casarella	1	192 Orzalli
	1 J. Niedzwecki	1	193 Olson
	1 Y.C. Whang	1	1932 Hoover
		1	1933 Lee
1	Harvard University	1	1933 Stefanowicz
	1 G.A. Baker	1	1942 Shen
		1	1942 Blake
1	Univ. of Illinois	1	1942 Bowers
	1 M.V. Morkovin	1	1942 Brown
		1	1942 Chandler
1	Penn State University	1	1942 DeMetz
	1 J.J. Eisenhuth	1	1942 Farabee
		1	1942 Geib
2	ARL, Penn State Univ.	1	1942 Gordon
	1 Dr. B. Parkin	1	1942 Granum
	1 Dr. R. Arndt	1	1942 Lewis
		1	1942 Mathews
2	Princeton University	1	1942 Paladino
	1 S.I. Cheng	1	1946 Spina
	1 G.L. Mellor	1	1946 Intolubbe
		30	5214.1 Report Distribution
3	Massachusetts Inst. of Tech.	1	522.1 Library (C)
	1 S.A. Orszag	1	522.2 Library (A)
	1 M.T. Landahl		
	1 P. Leehey		

DTNSRDC ISSUES THREE TYPES OF REPORTS

(1) DTNSRDC REPORTS, A FORMAL SERIES PUBLISHING INFORMATION OF PERMANENT TECHNICAL VALUE, DESIGNATED BY A SERIAL REPORT NUMBER.

(2) DEPARTMENTAL REPORTS, A SEMIFORMAL SERIES, RECORDING INFORMATION OF A PRELIMINARY OR TEMPORARY NATURE, OR OF LIMITED INTEREST OR SIGNIFICANCE, CARRYING A DEPARTMENTAL ALPHANUMERIC IDENTIFICATION.

(3) TECHNICAL MEMORANDA, AN INFORMAL SERIES, USUALLY INTERNAL WORKING PAPERS OR DIRECT REPORTS TO SPONSORS, NUMBERED AS TM SERIES REPORTS; NOT FOR GENERAL DISTRIBUTION.

END

FILMED

3 -86

DTIC